Research Article | Vol. 12, No. 3 / 1 Mar 2022 / Optical Materials Express 1122
Optical Materials EXPRESS

Effects of the polarization field on optical transitions and selection rules in Er doped GaN

YAQIONG YAN, JING LI, JINGYU LIN, AND HONGXING JIANG*

Department of Electrical and Computer Engineering, Texas Tech University, Lubbock, TX 79409, USA
**hx.jiang@ttu.edu*

Abstract: Effects of the polarization field on the Er^{3+} intra-4f shell transitions in GaN have been investigated via comparison of photoluminescence emission spectroscopy studies conducted on Er:GaN and Er:YAG. The dominant optical transitions were compared and analyzed. It was observed that the dominant optical transitions in Er:GaN/Er:YAG are between the Stark levels of the same/different irreducible representations. The unique selection rules in Er:GaN are a consequence of the presence of a net local polarization field acting on Er due to the wurtzite crystal structure of GaN. The results provide useful insights into understanding of the dominant optical transitions and the most probable emission lines to be utilized to achieve lasing in Er:GaN.

1. Introduction

Solid-state high energy laser (HEL) systems have various applications in communications, security, manufacturing, and health/medicine [1]. Neodymium doped YAG (Nd:YAG) emitting at 1.06 μm is the most common gain medium for solid-state HELs nowadays. However, the laser beam emitting at 1.06 μm can penetrate eye's lens onto the retina and it does not trigger the blink reflex and is thus rather dangerous to the eyes [2]. Compared to Nd:YAG, erbium doped YAG (Er:YAG) has an advantage of emitting at 1.5 μm [3–7]. This wavelength is strongly absorbed by the surface of the eye and is thus "eye-safe" [8]. However, the thermal properties of YAG are less desirable with a low thermal conductivity of $k \approx 14$ W/m·K and a large thermal expansion coefficient of $\alpha \approx 7 \times 10^{-6}$ °C^{-1} [9– 11], which limits its ability to remove the extra heat generated, and hence the power output. Among the emerging gain media for HELs under the current pursuit, with its superb optical, mechanical and thermal properties, erbium doped GaN (Er:GaN) has been recognized as a promising candidate, which not only emits at 1.5 μm, but GaN also possesses outstanding thermal properties, with a high thermal conductivity of $\kappa \approx 253$ W/m·K and low thermal expansion coefficient of $\alpha \approx 3.53 \times 10^{-6}$ °C^{-1} [12].

As gain media, GaN and YAG are two distinctly different hosts due to their different crystal structures. GaN possesses a wurtzite crystal structure. It is well known that the uniaxial nature of the GaN crystal causes a large spontaneous polarization field acting on its constituent atoms along the opposite direction of the c-axis [13]. In contrast, such an effect is absent in YAG because it has a cubic crystal structure. In Er:GaN, Er replaces Ga and hence is expected to experience a net polarization field. In contrast, such a local field does not exist, and the interaction potential is predominantly dipole type in Er:YAG. These two different types of interactions taking place in Er:GaN and Er:YAG will no doubt affect the selection rules of the Er intra-4f electron transitions, which is the focus of our studies here.

The Stark levels of the $^4I_{13/2}$ first excited state and $^4I_{15/2}$ ground state of the Er 4f shell and symmetry of Er in GaN determine the wavelengths of Er emission lines in the 1.5 μm spectral region. The Stark levels of $^4I_{13/2}$ and $^4I_{15/2}$ are indexed using a group theory with two representations Γ_4 and $\Gamma_{5,6}$ [14,15]. Understanding the selection rules of the intra-4f electron transitions between the $^4I_{13/2}$ first excited and the $^4I_{15/2}$ ground state of Er^{3+} in GaN host is critically important for determining the dominant emission lines for optical gain and lasing in Er:GaN. We report here for the first time the comparison studies of the photoluminescence

#448156 https://doi.org/10.1364/OME.448156
Journal © 2022 Received 1 Dec 2021; revised 26 Jan 2022; accepted 30 Jan 2022; published 17 Feb 2022

Optical Materials EXPRESS

(PL) emission spectroscopy carried out for Er:GaN and Er:YAG crystals, from which different selection rules of the Er intra-4f shell transitions in Er:GaN and Er:YAG have been identified. The results provide insightful knowledge for utilizing Er:GaN as a gain material for future solid-state HELs.

2. Experimental details

Er:GaN wafers of 2-inches in diameter with a thickness of 12 μm were grown by hydride vapor phase epitaxy (HVPE) on sapphire substrates. Prior to the deposition of Er:GaN, a GaN epilayer of about 3 μm in thickness was first grown by metal-organic chemical vapor deposition (MOCVD). For the subsequent HVPE growth of Er:GaN layer, the Er and Ga metals react with HCl gas, and the reactants were carried by hydrogen gas to the growth zone. The growth temperature was 1120°C, providing a growth rate of about 20 μm/h. The Er concentration in the Er:GaN samples of the present study is 3×10^{19} cm^{-3} (or 0.068%) as profiled by secondary ion mass spectroscopy (SIMS) measurements performed by Evans Analytical Group. The inset of Fig. 1 depicts the optical image of a representative Er:GaN wafer. At this doping concentration, the x-ray diffraction (XRD) rocking curve of the (0002) peak of the as-grown samples has a typical full width at half maxima (FWHM) of 1400 arcsec, whereas the θ–2θ scan measured at an orientation of 5° off from the c-axis revealed no observable peaks, which indicated that no polycrystalline structures are present and that the as-grown Er:GaN film is a single crystal [16]. However, the FWHM of the XRD rocking curve can be significantly decreased (to ~300 arcsec) if a fine mechanical polishing procedure is conducted [17]. For PL measurements, a laser diode emitting at $\lambda_{exc} = 405$ nm was used as an excitation source to provide a near band-edge excitation for Er:GaN. PL emission was collected using a fiber coupled monochromator and an InGaAs detector, providing an overall spectral resolution of 0.2 nm.

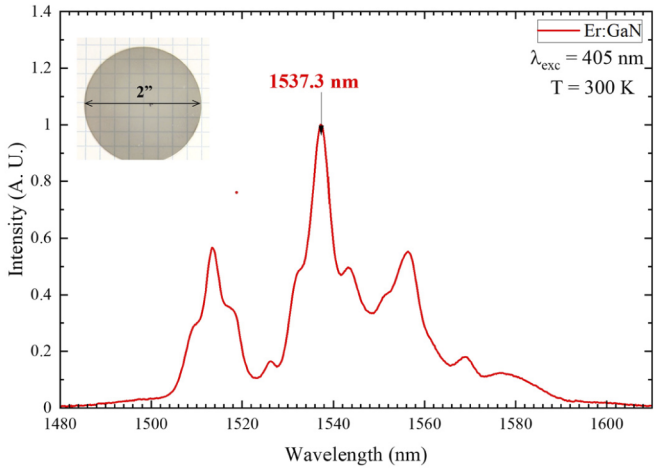

Fig. 1. PL emission spectrum measured in the wavelength range of 1480 to 1610 nm for an Er:GaN wafer grown by HVPE, excited by a laser diode emitting at λ_{exc} = 405 nm. The highest emission peak is at 1537.2 nm. The inset shows an optical image of an Er:GaN wafer of 2-inches in diameter used in the present study.

3. Results and discussion

A typical room temperature PL spectrum of Er:GaN measured in the 1.5 μm spectral range is shown in Fig. 1 resolving as many as 13 emission peaks, which results from the radiative Er intra-4f orbital transitions between different Stark levels of the 1st excited state ($^4I_{13/2}$) and the

Optical Materials EXPRESS

ground state ($^4I_{15/2}$). We noted that the Er emission spectral line shape of the as-grown samples reported here is almost identical to those of free-standing Er:GaN semi-bulk crystals (realized by laser-lift-off) [18]. Moreover, the measured room temperature Er emission spectral line shapes are similar regardless pumped by a resonant or band-edge excitation [18,19].

The Stark levels of the ground state ($^4I_{15/2}$) and the 1st excited state ($^4I_{13/2}$) of Er^{3+} in GaN have been deduced from the resolved spectral peaks in the PL spectrum in Fig. 1 together with a crystal field analysis [16] and are shown in Table 1. The top row in Table 1 indicates the 8 Stark levels of the $^4I_{15/2}$ ground state manifold, whereas the left-most column of Table 1 lists the 7 Stark levels of the $^4I_{13/2}$ 1st excited state. The values in parenthesis of Table 1 represent the Boltzmann population of the corresponding state levels. The values listed in the matrix element (i, j) are the emission wavelengths (in nm) and transition probabilities between the Stark level i of the $^4I_{13/2}$ 1st excited state and the Stark level j of the $^4I_{15/2}$ ground state. The energy levels deduced from the PL emission peaks agree well with those of the theoretical calculations [20]. The two irreducible representations of Γ_4 and $\Gamma_{5,6}$, are also listed for each Stark level. The expected emission wavelength of 1537.2 nm displayed in matrix elements (1,1) and (2,2) of Table. 1 resulting from transitions between states with the same irreducible representations ($\Gamma_4 \rightarrow \Gamma_4$, $\Gamma_{5,6} \rightarrow \Gamma_{5,6}$) highlighted in bold, matches perfectly with the observed dominant transition at 1537.2 nm in the PL spectrum shown in Fig. 1.

Table 1. The Stark levels of $^4I_{15/2}$ and $^4I_{13/2}$ of Er:GaN[a]

(nm) P (2j, (1-1i))	$^4I_{15/2}$ (cm^{-1})	**Γ_4** 4.7 (0.194)	**$\Gamma_{5,6}$** 10.2 (0.189)	**Γ_4** 39.1 (0.164)	**Γ_4** 111.0 (0.116)	**$\Gamma_{5,6}$** 156.2 (0.093)	**Γ_4** 168.9 (0.088)	**$\Gamma_{5,6}$** 187.9 (0.080)	**Γ_4** 196.2 (0.077)
$^4I_{13/2}$ (cm^{-1}) (1503 nm-1585 nm)	**Γ_4** 6510.1 (0.194)	**1537.2 (0.156)**	1538.5 (0.157)	1545.4 (0.162)	1562.7 (0.171)	1573.8 (0.176)	1577.0 (0.177)	1581.7 (0.178)	1583.8 (0.179)
	$\Gamma_{5,6}$ 6515.5 (0.189)	1535.9 (0.152)	**1537.2 (0.153)**	1544.1 (0.158)	1561.4 (0.167)	1572.5 (0.171)	1575.6 (0.172)	1580.4 (0.174)	1582.5 (0.174)
	Γ_4 6542.4 (0.166)	1529.6 (0.134)	1530.9 (0.134)	1537.7 (0.139)	1554.9 (0.146)	1565.9 (0.150)	1569.0 (0.151)	1573.7 (0.152)	1575.7 (0.153)
	Γ_4 6596.1 (0.128)	1517.1 (0.103)	1518.4 (0.104)	1525.1 (0.107)	1542.0 (0.113)	1552.8 (0.116)	1555.9 (0.117)	1560.5 (0.118)	1562.5 (0.118)
	$\Gamma_{5,6}$ 6613.0 (0.118)	1513.2 (0.095)	1514.5 (0.096)	1521.2 (0.099)	1538.0 (0.104)	1548.8 (0.107)	1551.8 (0.108)	**1556.4 (0.108)**	1558.4 (0.109)
	Γ_4 6636.2 (0.105)	1508.0 (0.085)	1509.2 (0.086)	1515.8 (0.088)	1532.5 (0.093)	1543.2 (0.096)	1546.2 (0.096)	1550.8 (0.097)	1552.8 (0.097)
	Γ_4 6663.2 (0.093)	1501.8 (0.075)	1503.1 (0.075)	1509.6 (0.077)	1526.2 (0.082)	1536.8 (0.084)	1539.8 (0.084)	1544.3 (0.085)	1546.3 (0.085)

[a]Note: The 8 Stark levels (top row) of the ground state ($^4I_{15/2}$) and the 7 Stark levels (left most column) of 1st excited state ($^4I_{13/2}$) of Er:GaN (cm^{-1}). The Boltzmann population of each Stark level at room temperature is listed in parenthesis, and the two irreducible representations of Γ_4 and $\Gamma_{5,6}$ are listed in bold. The transition wavelengths (nm) between the two Stark levels are shown in the matrix element, the calculated transition probabilities are indicated in parenthesis. The highlighted wavelength of 1537.2 nm in bold in matrix elements (1,1) and (2,2) matches with the dominant emission line at 1537.2 nm in Fig. 1. Wavelength 1556.4 nm highlighted in bold indicates the most likely candidate for achieving lasing under a resonant pumping at 1514 nm.

For a direct comparison, the room temperature PL emission spectrum of a commercially purchased 5% Er:YAG crystal (with its optical image shown in the inset of Fig. 2) was also measured and is plotted in Fig. 2. The highest emission peak is at 1533.2 nm. Based on the peak positions exhibited in the PL spectrum shown in Fig. 2 together with the crystal field analysis, the Stark levels of the ground state ($^4I_{15/2}$) and the 1st excited state ($^4I_{13/2}$) of Er^{3+} in YAG host crystal can also be constructed and are shown in Table 2. The expected transition lines listed at 1532.6 nm and 1533.7 nm in Table 2 highlighted in bold, resulting from transitions between states

Optical Materials EXPRESS

with different irreducible representations ($\Gamma_4 \rightarrow \Gamma_{5,6}$, $\Gamma_{5,6} \rightarrow \Gamma_4$), agree well with the dominant transition peak at 1533.2 nm observed in the PL spectrum of Fig. 2.

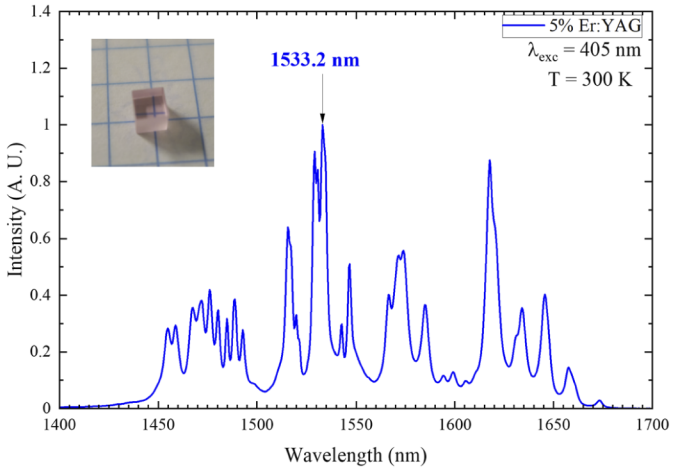

Fig. 2. PL emission spectrum measured in the wavelength range from 1400 to 1700 nm for an Er:YAG crystal, excited by a laser diode with a lasing wavelength at λ_{exc} = 405 nm. The highest emission peak is at 1533.2 nm. The inset depicts a photo of the Er:YAG sample used in the present study.

Table 2. The Stark levels of $^4I_{15/2}$ and $^4I_{13/2}$ of Er:YAG[a]

(nm) P(2j, (1-1i))	$^4I_{15/2}$ (cm^{-1})	**Γ_4** 0 (0.264)	**$\Gamma_{5,6}$** 19 (0.241)	**Γ_4** 57 (0.201)	**Γ_4** 76 (0.183)	**$\Gamma_{5,6}$** 411 (0.037)	**Γ_4** 424 (0.035)	**$\Gamma_{5,6}$** 523 (0.022)	**Γ_4** 568 (0.017)
$^4I_{13/2}$(cm^{-1}) (1503 nm-1585 nm)	**Γ_4** 6544 (0.276)	1528.1 (0.203)	**1532.6 (0.209)**	1541.5 (0.221)	1546.1 (0.225)	1630.5 (0.266)	1634.0 (0.266)	1660.9 (0.270)	1673.4 (0.271)
	$\Gamma_{5,6}$ 6596 (0.215)	1516.1 (0.158)	1520.5 (0.163)	1529.3 (0.172)	**1533.7 (0.176)**	1616.8 (0.207)	1620.2 (0.207)	1646.6 (0.210)	1658.9 (0.211)
	Γ_4 6602 (0.209)	1514.7 (0.154)	1519.1 (0.159)	1527.9 (0.167)	1532.3 (0.171)	1615.2 (0.201)	1618.6 (0.202)	1645.0 (0.204)	1657.3 (0.205)
	Γ_4 6779 (0.089)	1475.1 (0.066)	1479.3 (0.068)	1487.7 (0.071)	1491.9 (0.073)	1570.4 (0.086)	1573.6 (0.086)	1598.5 (0.087)	1610.0 (0.087)
	$\Gamma_{5,6}$ 6800 (0.081)	1470.6 (0.060)	1474.7 (0.061)	1483.0 (0.065)	1487.2 (0.066)	1565.2 (0.078)	1568.4 (0.078)	1593.1 (0.079)	1604.6 (0.080)
	Γ_4 6818 (0.074)	1466.7 (0.054)	1470.8 (0.056)	1479.1 (0.059)	1483.2 (0.060)	1560.8 (0.071)	1564.0 (0.071)	1588.6 (0.072)	1600.0 (0.073)
	Γ_4 6879 (0.055)	1453.7 (0.040)	1457.7 (0.042)	1465.8 (0.044)	1469.9 (0.045)	1546.1 (0.053)	1549.2 (0.053)	1573.3 (0.054)	1584.5 (0.054)

[a]Note: The Stark levels of the ground state ($^4I_{15/2}$) and the 1st excited state ($^4I_{13/2}$) of Er:YAG, including energy (cm^{-1}) of each Stark level, Boltzmann population, the irreducible representations Γ_4 and $\Gamma_{5,6}$. The highlighted wavelengths (bold) in matrix elements (1,2) and (2,4) correspond to the dominant emission line at 1533.2 nm in Fig. 2. At T = 0, only 8 emission lines are expected. At room temperature, more than 8 emission lines are observable because some of the levels within the $^4I_{13/2}$ excited state are thermally populated.

By carefully inspecting the PL spectra in Figs. 1 and 2 and analyzing data from Tables 1 and 2, we can conclude that the dominant transitions (emission peaks with highest intensities) in Er:GaN are between the Stark levels of the same representations $\Gamma_4 \rightarrow \Gamma_4$, and $\Gamma_{5,6} \rightarrow \Gamma_{5,6}$, whereas those in Er:YAG are between the Stark levels of different representations $\Gamma_4 \rightarrow \Gamma_{5,6}$ and

Optical Materials EXPRESS

$\Gamma_{5,6} \rightarrow \Gamma_4$. We believe that the difference in the selection rules observed in Er:GaN and Er:YAG can be accounted for by the local polarization fields acting on Er in wurtzite GaN [13]. The scenarios of local electric fields surrounding each Er atom due to the nearest neighbor atoms in both Er:GaN and Er:YAG are illustrated in Figs. 3(a) and (b), respectively. Due to the wurtzite crystal structure, electric fields acting on Er in GaN from the four nearest-neighbor nitrogen (N) atoms do not cancel out along the c-axis, resulting in a net polarization field acting upon the Er atom in the $[000\bar{1}]$ direction. In contrast, for Er in YAG, electric fields surrounding each Er atom from the eight nearest-neighbor oxygen (O) atoms counteract, resulting in a zero net field acting upon the Er atom. It is expected that this local polarization field will modify the Er intra-4f electron transitions. The actual potential and interaction of Er atoms in solids are very complicated. To focus on the main effects, we assume that the polarization field is dominant in Er in Er:GaN, whereas the dipole interaction is dominant with zero polarization field in Er:YAG.

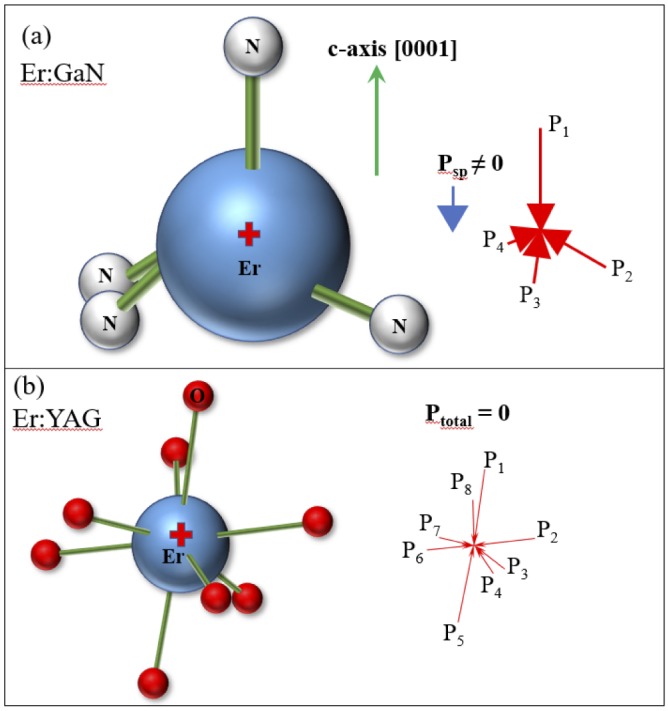

Fig. 3. (a) Illustration of local polarization fields acting on Er from four nearest-neighbor nitrogen (N) atoms in Er:GaN, resulting in a net polarization field acting on the Er atom pointing in the $[000\bar{1}]$ direction. (b) Local fields acting on Er in Er:YAG from eight nearest-neighbor oxygen (O) atoms, resulting in a zero net field on Er atom.

As such, the dominant local potential on Er atom due to dipole interaction in YAG has the form of $V(\mathbf{r}) = V(-\mathbf{r})$ [21]. However, due to the local polarization field, the local potential acting on the Er atom in GaN takes the form of

$$V(x) = V(-x),\ V(y) = V(-y),\ and\ V(z) = eEz\ or\ V(z) = -V(-z), \tag{1}$$

which is an even function in the x and y directions and an odd function in the z-direction. To simplify, by omit integrations for x and y components and keep only z component, the optical transition intensity of the Er atom is proportional to the integration or transition matrix element:

$$\begin{aligned} &V(x, y, -z) = -V(x, y, z) \\ &I = 0\ if\ f_{i,j}(x, y, -z) = \pm f_{i,j}(x, y, z), \end{aligned} \tag{2}$$

Optical Materials EXPRESS

where f_i and f_j are the wavefunctions of the initial (the $^4I_{13/2}$ 1st excited state) and final (the $^4I_{15/2}$ ground state) states of Er atoms. As such, our understandings for Er in GaN and YAG can be summarized as below:

(a) For dipole interaction in Er:YAG,

$$\begin{aligned} &V(x, y, -z) = V(x, y, z) \\ &I \neq 0 \; if \; f_{i,j}(x, y, -z) = \pm f_{i,j}(x, y, z), \end{aligned} \tag{3}$$

(b) For local polarization field in Er:GaN,

$$\begin{aligned} &V(x, y, -z) = -V(x, y, z) \\ &I = 0 \; if \; f_{i,j}(x, y, -z) = \pm f_{i,j}(x, y, z), \end{aligned} \tag{4}$$

Equations (3) and (4) clearly infer that Er:YAG and Er:GaN have different non-zero interaction matrix elements or different selection rules. Understanding these selection rules will help us to identify which emission lines in Er:GaN can potentially be utilized for lasing. For example, under 1514 nm resonant excitation, based on the selection rules in Er:GaN, the emission line at 1556 nm, which is an optical transition between the same representation $\Gamma_{5,6} \rightarrow \Gamma_{5,6}$, will be a probable candidate for achieving lasing.

From the PL results and Tables 1 and 2, the energy levels of the 1st excited state ($^4I_{13/2}$) and ground state ($^4I_{15/2}$) in Er:GaN and Er:YAG can also be constructed, and the results are shown in Fig. 4 with the symmetry representations of Γ_4 and $\Gamma_{5,6}$ being labeled in red and blue colors, respectively. The dominant transition lines of Er:GaN and Er:YAG are indicated. The difference in the selection rules in Er:GaN and Er:YAG can be readily recognized in Fig. 4. For Er:GaN, there should exist 4 transition lines between levels among the 2 lowest energy levels in both the first excited state ($^4I_{13/2}$) and the ground state ($^4I_{15/2}$). However, only 2 emission lines were observed experimentally: (i) from the second level of the $^4I_{13/2}$ to the second level of the $^4I_{15/2}$ ($\Gamma_{5,6} \rightarrow \Gamma_{5,6}$), and (ii) from the first level of the $^4I_{13/2}$ to the first level of the $^4I_{15/2}$ ($\Gamma_4 \rightarrow \Gamma_4$). These two emission lines both involve the states with the same irreducible representations ($\Gamma_4 \rightarrow \Gamma_4$ and $\Gamma_{5,6} \rightarrow \Gamma_{5,6}$). Another two emission lines between the 1st (2nd) level of the $^4I_{13/2}$ state to the 2nd (1st) level of $^4I_{15/2}$, which would have been ascribed to the transitions between states of different representation ($\Gamma_4 \rightarrow \Gamma_{5,6}$, $\Gamma_{5,6} \rightarrow \Gamma_4$), are absent. For Er:YAG, the situation is quite the opposite. Two transitions at 1532.6 and 1533.7 nm in Table 2 correspond to the dominant transition observed at 1533.2 nm of Fig. 2. However, these two transitions are both between different irreducible representations ($\Gamma_4 \rightarrow \Gamma_{5,6}$ and $\Gamma_{5,6} \rightarrow \Gamma_4$). These differences between Er:GaN and Er:YAG can be explained by different selection rules in Er:GaN and Er:YAG, as discussed above.

For PL spectra in Figs. 1 and 2, there are numerous emission lines observed in both Er:GaN and Er:YAG. There are many factors that determine the exact intensity of each emission line, such as Boltzmann population of each Stark level and transition rate. The selection rules discussed above have not only been applied to explain the emission lines with the highest intensities in Er:GaN and Er:YAG, but also the observable transition lines between the first excited state ($^4I_{13/5}$) and the ground state ($^4I_{15/2}$). The observations can be summarized as that the transition lines between the Stark levels of the same representations such as $\Gamma_4 \rightarrow \Gamma_4$ and $\Gamma_{5,6} \rightarrow \Gamma_{5,6}$ in Er:GaN in general have higher emission intensities in comparison with those between the Stark levels of different representations such as $\Gamma_4 \rightarrow \Gamma_{5,6}$ and $\Gamma_{5,6} \rightarrow \Gamma_4$ transitions, while the opposite is true in Er:YAG crystals.

It is worthwhile pointing out that the PL measurements are sensitive to the Er doping level and the crystalline quality in terms of the luminescent emission efficiencies. This is because there are two types of Er optical centers in Er:GaN, the isolated Er optical centers and the defect-related

Optical Materials EXPRESS

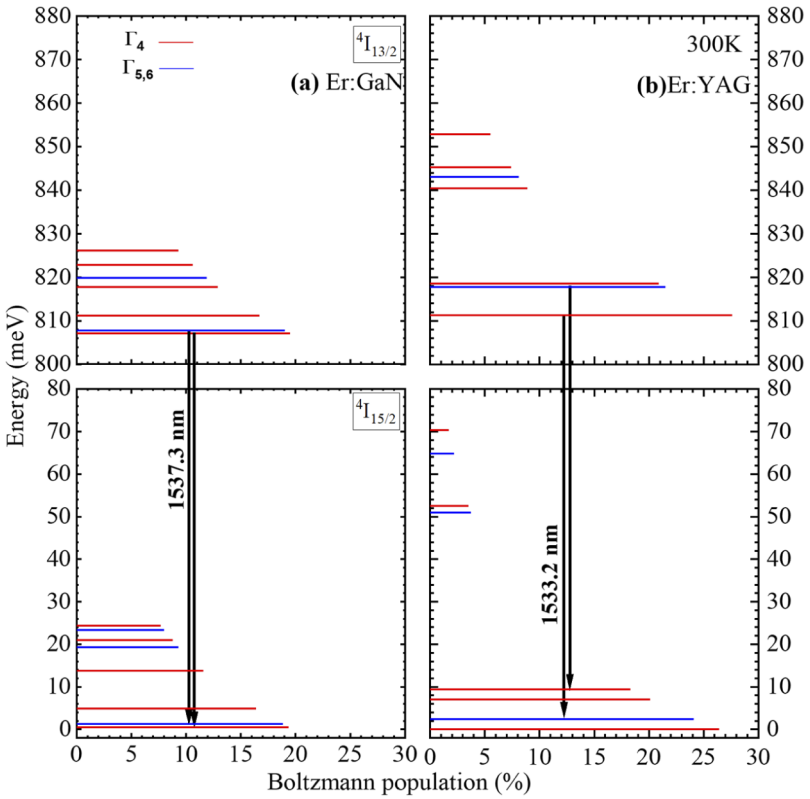

Fig. 4. The Stark energy level diagram of the $^4I_{13/2}$ first excited state and the $^4I_{15/2}$ ground state of Er^{3+} constructed from the PL spectra of Figs. 1 and 2 for Er:GaN and Er:YAG, respectively, with irreducible representation Γ_4 plotted in red lines, and $\Gamma_{5,6}$ plotted in blue lines.

center in Er:GaN [22]. While the emission wavelengths of the Er intra-4f orbital transitions are largely insensitive to the defect concentrations within the same host material [22–26], the quantum efficiency of the Er-defect centers is expected to be lower than that of the isolated Er centers because the energy transfer from excitation photons to the Er 4f shell is less efficient due to the presence of defects. Furthermore, the presence of defects will also increase optical loss. Therefore, improving the crystalline quality of Er:GaN is important to further enhance the efficiency of Er emission near 1.5 μm. However, the doping level and crystallinity of the host crystal will not alter the selection rule of the intra 4f shell transitions of the Er^{3+} ions within the same host crystal. Based on the realization of room temperature optical lasing and gain actions in Er:GaN epilayers under a band-to-band excitation [27,28], we believe that it is highly feasible to achieve lasing under a resonant excitation in Er:GaN semi-bulk crystals with further enhanced material quality and thicknesses.

4. Conclusion

In summary, PL emission spectra of both Er:GaN and Er:YAG crystals were measured and analyzed. The selection rules are found to be different for Er:YAG and Er:GaN due to their different crystalline structures. The energy levels in Er:GaN and Er:YAG were constructed and the most probable transition line for lasing emission in Er:GaN has been identified. Understanding

Optical Materials EXPRESS

the selection rule of the Er intra-4f orbital transitions in GaN is critical for further advancing Er:GaN crystals as an innovative gain medium for solid-state HELs.

Funding. Office of Naval Research Global (#N00014-17-1-2531).

Acknowledgements. H. X. Jiang and J. Y. Lin would like to acknowledge the support of Whitacre Endowed Chairs by the AT & T Foundation.

Disclosures. The authors declare no conflicts of interest.

Data Availability. The data that support the findings of this study are available within the manuscript.

References

1. Y. Kalisky and O. Kalisky, "The status of high-power lasers and their applications in the battlefield," Opt. Eng. **49**(9), 091003 (2010).
2. V. E. Kinsey, "Spectral transmission of the eye to ultraviolet radiations," Arch. Ophthalmol. **39**(4), 508–513 (1948).
3. C. B. Zachary, "Modulating the Er: YAG laser," Lasers Surg. Med. **26**(2), 223–226 (2000).
4. J. O. White, "Parameters for quantitative comparison of two-, three-, and four-level laser media, operating wavelengths, and temperatures," IEEE J. Quantum Electron. **45**(10), 1213–1220 (2009).
5. M. Němec, J. Šulc, L. Indra, M. Fibrich, and H. Jelínková, "Tunable eye-safe Er: YAG laser," Laser Phys. **25**(1), 015803 (2015).
6. T. Sanamyan, "Efficient cryogenic mid-IR and eye-safe Er: YAG laser," J. Opt. Soc. Am. B **33**(11), D1–D6 (2016).
7. D. J. Ottaway, L. Harris, and P. J. Veitch, "Short-pulse actively Q-switched Er: YAG lasers," Opt. Express **24**(14), 15341–15350 (2016).
8. J. A. Zuclich, D. J. Lund, and B. E. Stuck, "Wavelength dependence of ocular damage thresholds in the near-ir to far-ir transition region: proposed revisions to MPES," Health Phys. **92**(1), 15–23 (2007).
9. R. Wynne, J. L. Daneu, and T. Y. Fan, "Thermal coefficients of the expansion and refractive index in YAG," Appl. Opt. **38**(15), 3282–3284 (1999).
10. H. Furuse, R. Yasuhara, and K. Hiraga, "Thermo-optic properties of ceramic YAG at high temperatures," Opt. Mater. Express **4**(9), 1794–1799 (2014).
11. W. Xie, S.-C. Tam, H. Yang, J. Gu, G. Zhao, Y. L. Lam, and W. Tan, "Heat transfer for diode side-pumped YAG slabs," Optics & Laser Technol. **31**(7), 521–528 (1999).
12. H. Shibata, Y. Waseda, H. Ohta, K. Kiyomi, K. Shimoyama, K. Fujito, H. Nagaoka, Y. Kagamitani, R. Simura, and T. Fukuda, "High thermal conductivity of gallium nitride (GaN) crystals grown by HVPE process," Mater. Trans. **48**(10), 2782–2786 (2007).
13. J. P. Ibbetson, P. T. Fini, K. D. Ness, S. P. DenBaars, J. S. Speck, and U. K. Mishra, "Polarization effects, surface states, and the source of electrons in AlGaN/GaN heterostructure field effect transistors," Appl. Phys. Lett. **77**(2), 250–252 (2000).
14. G.F. Koster, J.O. Dimmock, R.G. Wheeler, and H. Statz, *Properties of the Thirty-two Point Groups* (MIT Press, 1963), pp. 55–57.
15. R. Maâlej, M. Dammak, S. Kammoun, and M. Kammoun, "Theoretical investigation of a single erbium center in hexagonal gallium nitride," J. Lumin. **126**(2), 695–701 (2007).
16. Y. Q. Yan, T. B. Smith, J. Li, J. Y. Lin, and H. X. Jiang, "Erbium energy levels in GaN grown by hydride vapor phase epitaxy," AIP Adv. **10**(12), 125006 (2020).
17. Z. Y. Sun, J. Li, W. P. Zhao, J. Y. Lin, and H. X. Jiang, "Toward the realization of erbium-doped GaN bulk crystals as a gain medium for high energy lasers," Appl. Phys. Lett. **109**(5), 052101 (2016).
18. Z. Y. Sun, Y. Q. Yan, W. P. Zhao, J. Li, J. Y. Lin, and H. X. Jiang, "Resonant excitation cross-sections of erbium in freestanding GaN bulk crystals," Appl. Phys. Lett. **112**(20), 202103 (2018).
19. Z. Y. Sun, L. C. Tung, W. P. Zhao, J. Li, J. Y. Lin, and H. X. Jiang, "Excitation and emission mechanisms of Er: GaN gain medium in 1.5 μm region," Appl. Phys. Lett. **111**(7), 072109 (2017).
20. M. Stachowicz, A. Kozanecki, C. G. Ma, M. G. Brik, J. Y. Lin, H. X. Jiang, and J. M. Zavada, "Crystal field analysis of rare-earth ions energy levels in GaN," Opt. Mater. **37**, 165–174 (2014).
21. Ł. Dobrzycki, E. Bulska, D. A. Pawlak, Z. Frukacz, and K. W. Niak, Inorganic chemistry, "Structure of YAG crystals doped/substituted with erbium and ytterbium," Inorg. Chem **43**(24), 7656–7664 (2004).
22. V. X. Ho, T. V. Dao, H. X. Jiang, J. Y. Lin, J. M. Zavada, S. A. McGill, and N. Q. Vinh, "Photoluminescence quantum efficiency of Er optical centers in GaN epilayers," Sci Rep **7**(1), 1–7 (2017).
23. R. G. Wilson, R. N. Schwartz, C. R. Abernathy, S. J. Pearton, N. Newman, M. Rubin, T. Fu, and J. M. Zavada, "1.54-μm photoluminescence from Er-implanted GaN and AlN," Appl. Phys. Lett. **65**(8), 992–994 (1994).
24. A. J. Steckl and J. M. Zavada, "Optoelectronic properties and applications of rare-earth-doped GaN," MRS Bull. **24**(9), 33–38 (1999).
25. V. Dierolf, in *Rare-Earth Doped III-Nitrides for Optoelectronic and Spintronic Applications*, edited by K. O'Donnell and V. Dierolf, eds. (Canopus Academic Publishing Ltd.; Springer SBM, 2010), Chap. 8.
26. A. Braud, in *Rare-Earth Doped III-Nitrides for Optoelectronic and Spintronic Applications*, edited by K. O'Donnell and V. Dierolf, eds. (Canopus Academic Publishing Ltd. Springer SBM, 2010), Chap. 9.

Optical Materials EXPRESS

27. V. X. Ho, T. M. Al tahtamouni, H. X. Jiang, J. Y. Lin, J. M. Zavada, and N. Q. Vinh, "Room-temperature lasing action in GaN quantum wells in the infrared 1.5 μm region," ACS Photonics **5**(4), 1303–1309 (2018).
28. V. X. Ho, Y. Wang, B. Ryan, L. Patrick, H. X. Jiang, J. Y. Lin, and N. Q. Vinh, "Observation of optical gain in Er-doped GaN epilayers," J. Lumin. **221**, 117090 (2020).